Asian Pub. Corp.

www.asianpubs.org

ARTICLE

Non-Nucleoside HIV-1 Reverse Transcriptase Inhibition Activity of a Series of Dihydroalkoxybenzyloxopyrimidine (DABO) Derivatives: CoMFA, CoMSIA and Docking Studies

Bikash Kumar Sarkar[1], Ananda Sarkar[2] and Atish Dipankar Jana[3,✉]

Asian Journal of Organic & Medicinal Chemistry

Volume: 5 Year: 2020
Issue: 3 Month: July–September
pp: 265–272
DOI: https://doi.org/10.14233/ajomc.2020.AJOMC-P289

Received: 27 August 2020
Accepted: 12 September 2020
Published: 15 September 2020

ABSTRACT

CoMFA, CoMSIA and molecular docking studies have been carried out for a set of 42 dihydroalkoxybenzyloxopyrimidine (DABO) derivatives for which anti-HIV activity values are available. In 3D-QSAR studies-comparative molecular field analysis (CoMFA) as well as comparative molecular similarity indices analysis (CoMSIA) have been performed. Both the QSAR model nicely explains the inhibitory activities of DABO derivatives as well as provides molecular level insights revealing which regions in 3D space around the molecules are more important for their anti HIV-activities. These models have a quite high square correlation coefficient (r^2 = 0.817 for CoMFA and r^2 = 0.943 for CoMSIA). A docking study of the highest active molecule into the binding site of the protein HIV-1 RT (PDB ID-1RT1) shows that hydrogen bonding between pyrimidine moiety of the ligand and the Lysine-101 moiety along with Valine-106 moiety of the HIV protein play most important role for stabilizing the ligand in the binding pocket of the protein.

KEYWORDS

HIV, Dihydroalkoxybenzyloxopyrimidine, CoMFA, CoMSIA, Docking studies.

INTRODUCTION

HIV-1 is a retrovirus that attacks the human immune system and causes acquired immunodeficiency syndrome (AIDS) [1]. This virus replicates through the action of resverse transcriptase (RT) enzyme. Drugs available today for treating AIDS are designed to inhibit the functioning of the reverse transcriptase enzyme. Drugs for preventing AIDS are broadly classified into two categories *viz*. nucleoside reverse transcriptase inhibitors (NRTIs) and non-nucleoside inhibitors [2]. 3′-Azidomythidine (AZT) [3] is an example of the nucleoside inhibitor, whereas, HEPT [4] and TIBO [5] are currently available non-nucleoside inhibitors. Drugs belonging to both categories are beset with problems of cytotoxicity and drug-resistance [6]. Thus quest for better drug molecules to restrain the activity of HIV-1 retrovirus is still an ongoing challenge. Molecules, based on dihydroalkoxybenzyloxopyrimidines (DABO) have been reported to exhibit efficient anti HIV-1 activity [7].

Author affiliations:

[1]Department of Physics, Mrinalini Datta Mahavidyapith, Birati, Kolkata-700051, India
[2]Department of Physics, Acarya Prafulla Chandra College, Kolkata-700131, India
[3]Department of Physics, Behala College, Parnasree, Kolakata-700060, India

✉To whom correspondence to be addressed:

E-mail: atishdipankarjana@yahoo.in

Available online at: http://ajomc.asianpubs.org

Successful design of effective drug molecules is fundamentally dependent on the clear understanding of the electronic nature and its correlation among the members of a closely related set of molecules. This in turn leads to the relative importance of the steric, electrostatic, hydrophobic, van der Waals and hydrogen bond donor-acceptor functionality in the chosen set of molecules. Three dimensional quantitative structure activity relationship (3D-QSAR) is a well established methodology in the field of rational drug design which provides a mathematical relationship between the activities and interaction fields for a given set of molecules [8,9]. This relationship (the QSAR equation) in essence, captures the common chemical characteristics of the set of molecules towards their inhibitory activities.

In present study, a comparative molecular field analysis (CoMFA) [10] and a comparative molecular similarity indices analysis (CoMSIA) [11,12] have been carried out for a set of 42 closely related DABO derivatives that correlate their HIV-1 reverse transcriptase inhibition activities with their electronic and structural features. The derived 3D-QSAR models have provided detailed molecular level insights regarding the relevant interacting fields and the corresponding regions over the molecular surface where these interactive fields are operative.

Docking studies have also been performed that have provided a valuable information regarding the nature of intermolecular interactions and mode of binding of the highest active molecule in the binding site of the relevant HIV-1 RT protein (PDB ID: 1RT1.pdb) [13-15]. Docking studies have been carried out using the Surflex-Dock module of Sybyl-X software package [16].

EXPERIMENTAL

Selection of dataset: Anti HIV activity data of a series of DABO derivatives have been taken from published literature [17-20]. Activity values for a set of 42 molecules collected from these sources have been listed in Table-1. In these studies, the biological profile of the molecules were evaluated in HIV-1 RT affinity binding assays using [^{3}H]-dGTP as the radioligand. IC_{50} values of the molecules were transformed into $\log(1/IC_{50})$, abbreviated as pIC_{50}. This pIC_{50} values range from 4.23 M to 6.70 M.

Out of 42 DABO derivatives, 34 molecules were chosen for the training set and others were used as test set. The constitution of test set was based on the consideration that the molecules belonging to the test set span the whole activity range evenly and also the test set is the true representative of the chemical and structural diversity of the whole dataset. External predictivity of the resulting QSAR model was tested for the molecules belonging to this test set.

3D-QSAR (CoMFA and CoMSIA) analysis

Alignment of molecules: Alignment of the relevant set of molecules is an important part of the development of successful CoMFA and CoMSIA models [21]. In present study, ligand based alignment technique has been chosen. In the ligand based

TABLE-1
CHEMICAL STRUCTURE AND HIV-1 REVERSE TRANSCRIPTASE
NON-NUCLEOSIDE INHIBITION ACTIVITY DATA OF DABO DERIVATIVES

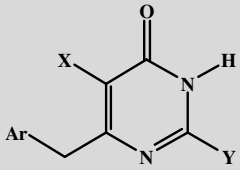

No.	X	Ar	Y	pIC_{50}	No.	X	Ar	Y	pIC_{50}
1#	Me	2-Naphthyl	S-*sec*-Bu	4.23	22	H	Ph	S-Cyclopentyl	5.55
2#	H	1-Naphthyl	S-Cyclopentyl	4.31	23	H	3-Me-Ph	S-Cyclopentyl	5.59
3	Me	1-Naphthyl	S-Cyclopentyl	4.35	24#	Me	3-Me-Ph	S-Me	5.60
4	Me	4-F-Ph	S-*sec*-Bu	4.59	25	Me	3-Me-Ph	S-*iso*-Pr	5.60
5	Me	4-Cl-Ph	S-*sec*-Bu	4.77	26	Me	3-Me-Ph	S-Cyclohexyl	5.66
6	H	1-Naphthyl	S-*sec*-Bu	4.79	27	Me	Ph	S-*tert*-Bu	5.72
7	H	2-Naphthyl	S-*sec*-Bu	4.83	28	Me	2,6-di-Cl-Ph	S-Cyclopentyl	5.80
8#	H	4-Cl-Ph	S-*sec*-Bu	5.02	29	H	2,6-di-Cl-Ph	S-*iso*-Pr	5.89
9	H	3-Me-Ph	4-*tert*-Ph	5.09	30	Me	2,6-di-Cl-Ph	S-*iso*-Pr	5.94
10#	Me	2,6-di-Cl-Ph	S-Cyclohexyl	5.31	31	Me	2,6-di-Cl-Ph	S-*n*-Pr	5.94
11	Me	Ph	S-Me	5.31	32	Me	2,6-di-Cl-Ph	S-*tert*-Pr	5.96
12	Me	Ph	S-*sec*-Bu	5.32	33#	H	2,6-di-F-Ph	S-Me	6.10
13	Me	3-Me-Ph	S-*tert*-Bu	5.34	34	Me	2-Cl-Ph	S-*sec*-Bu	6.10
14	Me	Ph	S-Cyclohexyl	5.37	35	Me	2-F-Ph	S-*sec*-Bu	6.10
15	H	3-Cl-Ph	S-*sec*-Bu	5.42	36#	Me	3-NO_2-Ph	S-*sec*-Bu	6.10
16	Me	3-Me-Ph	S-Cyclohexyl	5.47	37	H	2-F-Ph	S-*sec*-Bu	6.22
17	H	2-Cl-Ph	S-*sec*-Bu	5.49	38	H	3-NO_2-Ph	S-*sec*-Bu	6.22
18	Me	3-F-Ph	S-*sec*-Bu	5.52	39	H	2,6-di-Cl-Ph	S-*tert*-Bu	6.22
19#	H	2,6-di-Cl-Ph	S-Me	5.52	40	H	2,6-di-Cl-Ph	S-*n*-Bu	6.30
20	H	Ph	S-Cyclohexyl	5.52	41	H	2,6-di-Cl-Ph	S-Cyclopentyl	6.40
21	H	3-Me-Ph	S-*iso*-Pr	5.54	42	H	2,6-F-Cl-Ph	S-*n*-Bu	6.70

#Molecules belonging to test set

alignment, first a template molecule is isolated and then the remaining molecules are aligned over this. Here molecule no. 42 showing the highest activity has been chosen as the template molecule. The aligned set of molecules has been depicted in Fig. 1.

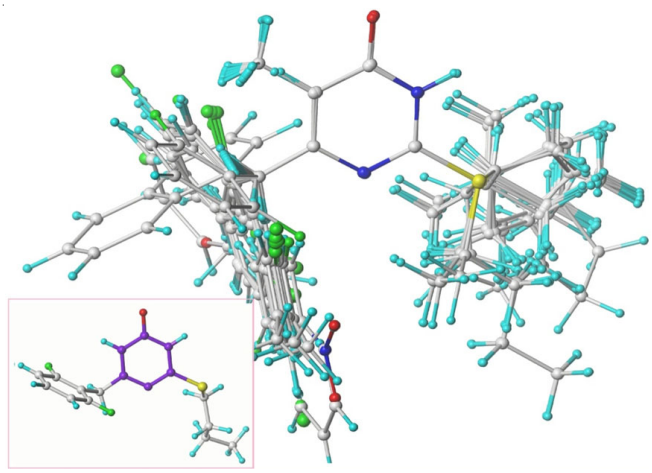

Fig. 1. Molecules have been aligned over the template molecule 42 which is shown in the inset. The common moiety is pyrimidine ring (marked purple)

CoMFA and CoMSIA setup: Both CoMFA and CoMSIA models have been built separately based on the aligned set of molecules as described earlier. A 3D cubic lattice has been taken to generate the CoMFA and CoMSIA molecular descriptor fields. The grid spacing of the 3D cubic lattice was taken to be 1 Å. This lattice extended 4 Å beyond the aligned set of molecules in every direction. Tripos force field was utilized to calculate the van dar Waals potential as well as the Coulombic potentials. A sp^3 hybridized carbon atom bearing +1 charge was taken as the probe atom for calculating the steric and the electrostatic fields in the CoMFA model. Truncation limit for energy values were set at 30 kcal/mol. In the CoMSIA method we have used the same lattice box. A probe atom having radius 1.0 Å with charge +1 was utilized for integration of steric, hydrophobic, electrostatic, hydrogen bond donor and hydrogen bond acceptor fields. Both hydrophobic as well as hydrogen bond properties were set at +1. Attenuation factor was taken to be 0.3, which is the default value in Sybyl-X software [16].

Derivation and validation of the model: Partial least squares (PLS) were used to find the linear relationship between the CoMFA fields and the pIC_{50} values. Another linear relationship was established between CoMSIA fields and pIC_{50} values in a similar manner. Leave-one-out (LOO) method was the basis of cross-validation analysis. The general procedure adopted here is to remove one molecule from the data set and predict its activity from a model based on the rest of the data set [22]. For determining optimum number of components (ONC), PLS was combined with the cross-validation option. ONC were then used in deriving the final CoMFA and CoMSIA model without cross-validation. ONC is the number of components resulting in highest cross-validated correlation coefficient (r^2_{cv} or q^2). In the cross-validation procedure a default value of 2.0 kcal/mol was set for column filtering. Non-cross-validated analysis with the ONC was used to derive the final models along with its correlation coefficient r^2. A test set of seven molecules not included in the training set was employed to test the predictive abilities of the model. For predicting the pIC_{50} values, these seven molecules were aligned to the template molecule. Eqn. 1 was employed to compute the predictive correlation coefficient (r^2_{pred}), based on the molecules of the test set.

$$r^2_{pred} = 1 - \frac{\sum (Y_{obs(test)} - Y_{pred(test)})^2}{\sum (Y_{obs(test)} - \bar{Y}_{training})^2} \quad (1)$$

here $Y_{pred(test)}$ and $Y_{obs(test)}$ are the predicted and observed activity values of the test set molecules. $\bar{Y}_{training}$ indicates the mean activity value of the training set molecules. The value of r^2_{pred} for an acceptable model should be greater than 0.5 [23].

Molecular docking: To investigate the protein-ligand interactions, molecule 42 having the highest experimental activity value was selected as a reference and docked into the binding site of HIV-1 RT (PDB ID: 1RT1.pdb) using Surflex-Dock module of Sybyl-X package [16]. The Surflex uses an empirical scoring function and a patented search engine to dock ligand into the receptor's binding site. Crystal structure of HIV-1 RT (1RT1) complexed with MKC-442 (resolution value is 2.55 Å) obtained from the Protein Data Bank has been used for docking studies as the original ligand of MKC-442 is very similar in structure to our dataset. The HIV-1 RT structure was utilized in subsequent docking experiments without energy minimization. All ligands and water molecules have been removed and the polar hydrogen atoms were added. Protomol was established using the 'ligand' option in Sybyl-x, which finds the ligand location in the same coordinate space as in the receptor. To visualize the binding mode between the protein and ligand, the molecular computer aided design (MOLCAD) program, implemented in Sybyl-X [16], was employed.

RESULTS AND DISCUSSION

3D-QSAR model: The statistical parameters corresponding to the CoMFA model has been listed in Table-2. The CoMFA model of the DABO derivatives has a good correlation coefficient (q^2) 0.673 with an optimized component of 4, which suggests that the model should be a valuable tool for predicting the pIC_{50} values. A high non-cross-validated correlation coefficient (r^2) of 0.817 with a low standard error estimate (SEE) of 0.247, F value of 32.402 and predictive correlation coefficient ($r_{pred}{}^2$) value 0.668 have been obtained. Steric and electrostatic contri-butions surrounding the aligned set of molecules were found to be 0.525 and 0.475, respectively. The actual pIC_{50}

TABLE-2
PLS RESULTS OF CoMFA AND CoMSIA MODELS

PLS Statistics	CoMFA	CoMSIA
q^2	0.673	0.695
r^2	0.817	0.943
r^2_{pred}	0.668	0.684
ONC	4	5
SEE	0.247	0.140
F Value	32.402	93.047
Field contributions		
Steric	0.525	0.437
Electrostatic	0.475	0.563

TABLE-3
PREDICTED ACTIVITY VALUES FROM THE CoMFA AND CoMSIA MODELS

S. No.	Obsd Act	CoMFA		CoMSIA		S. No.	Obsd Act	CoMFA		CoMSIA	
		Pred Act	Res	Pred Act	Res			Pred Act	Res	Pred Act	Res
01#	4.23	4.90	0.67	4.73	0.50	22	5.55	5.48	-0.07	5.460	-0.09
02#	4.31	5.06	0.75	5.06	0.75	23	5.59	5.45	-0.14	5.481	0.11
03	4.35	4.56	0.21	4.57	0.22	24#	5.60	5.79	0.19	6.107	0.51
04	4.59	4.54	-0.05	4.59	0.00	25	5.60	5.57	-0.03	5.379	-0.22
05	4.77	4.81	0.04	4.63	-0.14	26	5.66	5.63	-0.03	5.595	-0.07
06	4.79	4.65	-0.13	4.65	-0.14	27	5.72	5.61	-0.11	5.584	-0.14
07	4.83	5.07	0.24	4.82	0.00	28	5.80	5.85	0.05	5.907	0.11
08#	5.02	5.06	0.04	5.00	-0.02	29	5.89	6.20	0.31	6.131	0.24
09	5.09	5.21	0.12	5.31	0.22	30	5.94	5.91	-0.03	5.884	-0.06
10#	5.31	5.50	0.19	5.17	-0.14	31	5.94	5.99	0.05	5.982	0.04
11	5.31	5.40	0.09	5.45	0.14	32	5.96	6.03	0.07	5.969	0.01
12	5.32	5.35	0.03	5.38	0.06	33#	6.10	6.08	-0.02	6.291	0.19
13	5.34	5.39	0.05	5.39	0.05	34	6.10	6.05	-0.05	6.059	-0.04
14	5.37	5.56	0.19	5.54	0.17	35	6.10	6.09	-0.01	5.957	-0.14
15	5.42	5.37	-0.05	5.45	0.03	36#	6.10	5.54	-0.56	6.543	0.44
16	5.47	5.49	0.02	5.50	0.03	37	6.22	6.25	0.030	6.021	-0.20
17	5.49	5.90	0.41	5.84	0.35	38	6.22	6.13	-0.09	6.225	0.01
18	5.52	5.62	0.104	5.47	-0.05	39	6.22	6.32	0.104	6.266	0.046
19#	5.52	5.83	0.31	5.20	-0.32	40	6.30	6.27	-0.03	6.272	-0.03
20	5.52	5.54	0.02	5.50	-0.03	41	6.40	6.23	-0.17	6.252	-0.15
21	5.54	5.49	-0.05	5.45	-0.10	42	6.70	5.61	-1.09	6.671	-0.03

#Molecules belonging to test set

values of the training set and the test set along with the predicted pIC_{50} values given by the CoMFA model is given in Table-3 and the graph of actual activity *versus* predicted pIC_{50} values of the molecules is depicted in Fig. 2.

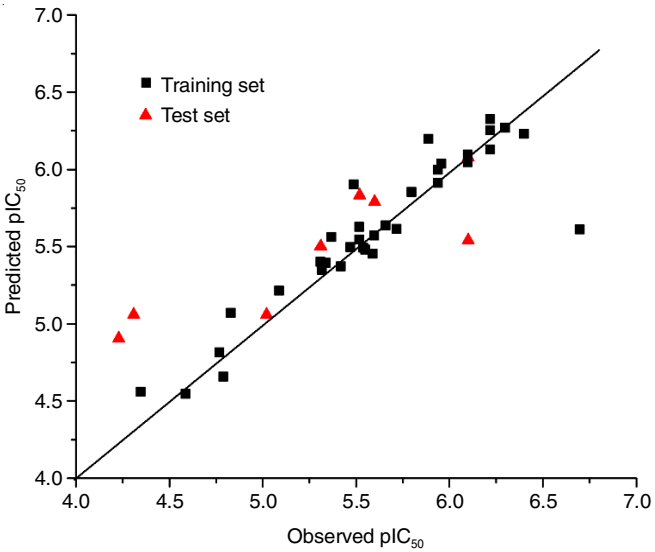

Fig. 2. Observed *versus* the predicted activity values following the CoMFA model

In CoMSIA model, five CoMSIA descriptors in different combinations change the model significance and predictivity. For this reason, all 31 possible descriptors' combinations were calculated with associated parameters. The best CoMSIA model, based on Steric and Electrostatic fields has the highest q^2 value (0.695) and a high non-cross-validated correlation coefficient r^2 of 0.943 with a low SEE value of 0.140 and F value of 93.047. Contributions of Steric and Electrostatic fields were 0.437 and 0.563, respectively. All the statistical parameters for the CoMSIA model have been listed in Table-2. The actual pIC_{50} values of the training set and the test set along with the predicted pIC_{50} values given by the CoMFA model is given in Table-3 and the graph of actual activity *versus* predicted pIC_{50} values of the molecules is depicted in Fig. 3.

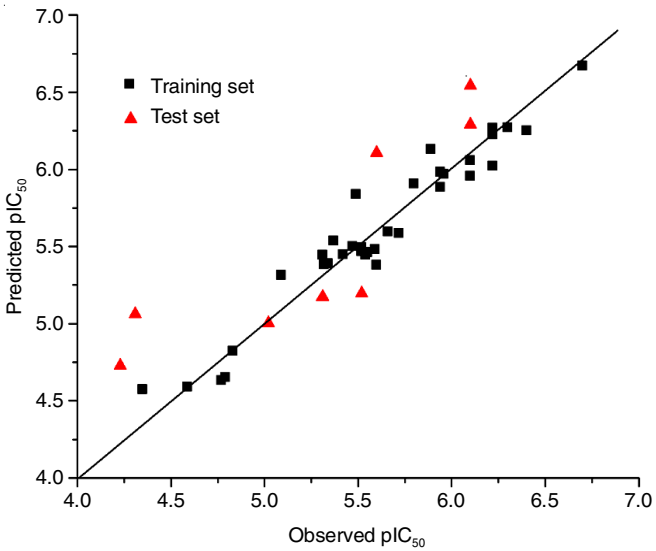

Fig. 3. Observed *versus* the predicted activity values following the CoMSIA model

The calculated results of the external validation for CoMFA and CoMSIA models have been listed in Table-2. It was shown by this external validation that both the model posses high predictive power and are reliable for predicting the activities of new molecules.

Interpretation of the 3D-QSAR model: To visualize the information content of the derived 3D-QSAR model, CoMFA contour maps were generated to rationalize the regions in 3D

space around the molecules where changes in the steric and electrostatic fields would affect the activity in a positive or in a negative way. The CoMFA steric and electrostatic contour maps have been shown in Figs. 4 and 5, respectively. The steric field is represented by green and yellow contours, in which green contours indicate regions where bulky group would be favourable, while the yellow contours represent regions where bulky group would decrease the activity. Molecule #42 was selected as a reference structure. As shown in Fig. 4, in the CoMFA steric map the yellow contours are located near the substitution X on the central ring and the green contours surround the –Ar group attached to the central ring. This indicates that less bulky substituents at the position of X will favour the anti HIV activity and more bulky substituents at the position of Ar will increase the anti-HIV activity. As can be seen from Table-1, this is the general trend of the activity data, molecule 37 to 42 all of which has X=H show relatively higher activity values. Similarly for the molecules 38 to 42 where there are double substitution of the –Ar moiety, show relatively higher anti HIV activity.

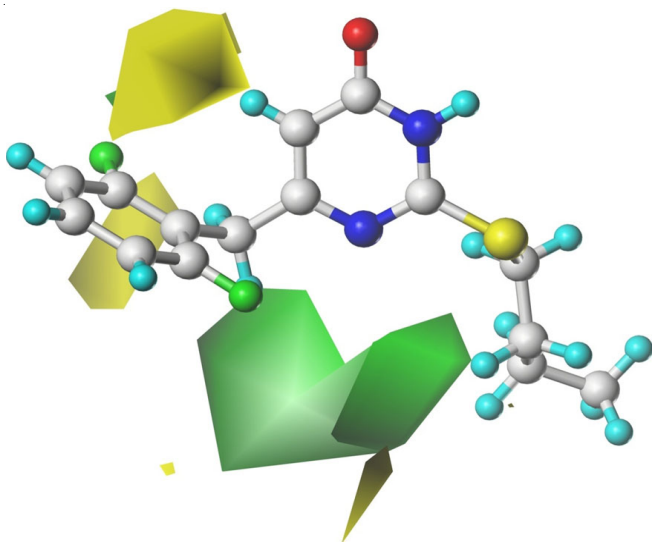

Fig. 4. CoMFA Steric field. Green contours favour bulky groups for higher activity and yellow contours favour less bulky groups for higher activity

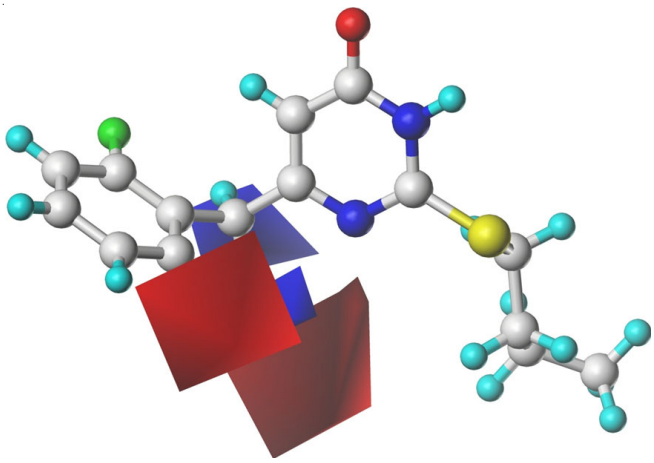

Fig. 5. CoMFA Electrostatic contour maps. Blue contours represent regions where positive charge will favour activity and red contours represent regions where excess negative charge will favour activity

The CoMSIA steric contour maps (Fig. 6) also has more or less similar nature to the CoMFA steric fields (Fig. 4). CoMSIA model shows that the bulky substituent at the periphery of Ar group and at the position of the Y substituent on the central ring is favourable for the better activity.

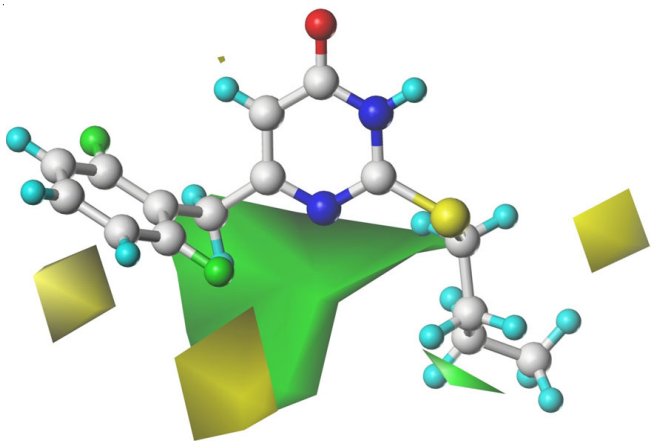

Fig. 6. CoMSIA Steric field. Green contours favour bulky groups for higher activity and yellow contours favour less bulky groups for higher activity

The electrostatic contour maps are also nearly identical in both the cases of CoMFA and CoMSIA models (Figs. 5 and 7). In the CoMFA electrostatic map the large blue contours surround the X and Ar regions away from the molecule and a small red contour lie close to the Ar group. This indicates that the electropositive regions on the binding protein will act as suitable donor for the electronegative acceptor regions on the molecule. Small red contours also indicate that increase of the negative charge concentration on the periphery of the Ar group and at the Y position will favour the increased anti HIV activity. In the CoMSIA electrostatic contour map (Fig. 7) prominent red contours around the lower region of the –Ar group indicates the possibility of designing better anti-HIV active molecules by increasing the negative charge concentration at the periphery of –Ar moiety and blue contour around the central core indicates electron withdrawing substituents on it will make it more positive and is likely to increase the anti-HIV activity. Molecule

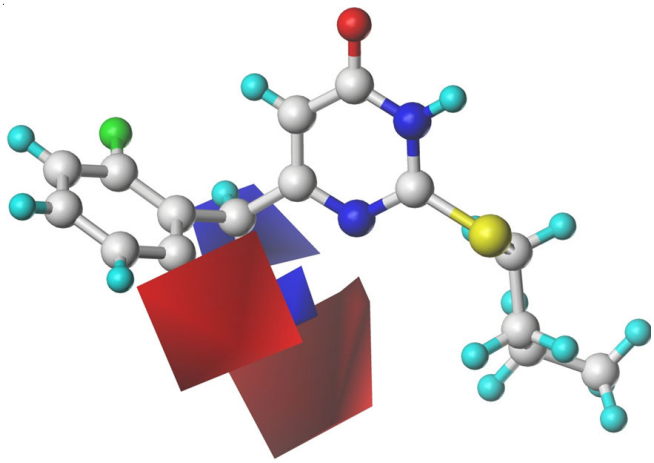

Fig. 7. CoMSIA Electrostatic field. Blue contours represent regions where positive charge will favour activity and red contours represent regions where excess negative charge will favour activity

39 to 42, for which there are two chloro substitutions on the –Ar moiety, show higher activity as this increases the negative charge concentration on the –Ar ring. These chlorine atoms are likely to act as donor in the interaction with the protein moieties.

Molecular docking: The binding mode of molecule 42 with 1RT1 protein, obtained from docking analysis is shown in Fig. 8. The pyrimidine moity play decisive role in establishing a cyclic hydrogen bonding motif with the Lysine 101 residue. The pyrimidine moiety and the Lysine group are complementary to each other, each having a NH donor group and C=O acceptor group. A $R_2^2(9)$ cyclic hydrogen bonding synthon [24] is established between these two. The N···O distance between the N donor of Lysine 101 and O acceptor atom of the pyrimidine moiety is 3.192 Å, H···O distance is 2.273 Å and the <NH···O angle is 152.17°. On the other hand the N···O distance between the N donor of the pyrimidine moiety and O acceptor atom of Lysine 101 is 2.735 Å, the H···O distance is 1.800 Å and the <NH···O angle is 161.59°. There is a further hydrogen bonding between the pyrimidine moiety the Valine 106 residue in which pyrimidine N atom act as the acceptor for the CH donor from the Valine 106 residue. C···N distance is 3.664 Å, H···N distance is 2.948 Å and <CH···N angle is 122.93°. It is to be noted that the above mentioned cyclic hydrogen bonding pattern is a generic feature between the DABO class of ligands and the 1RT1 protein (Fig. 8) as the common pyrimidine scaffold is involved in this hydrogen bonding.

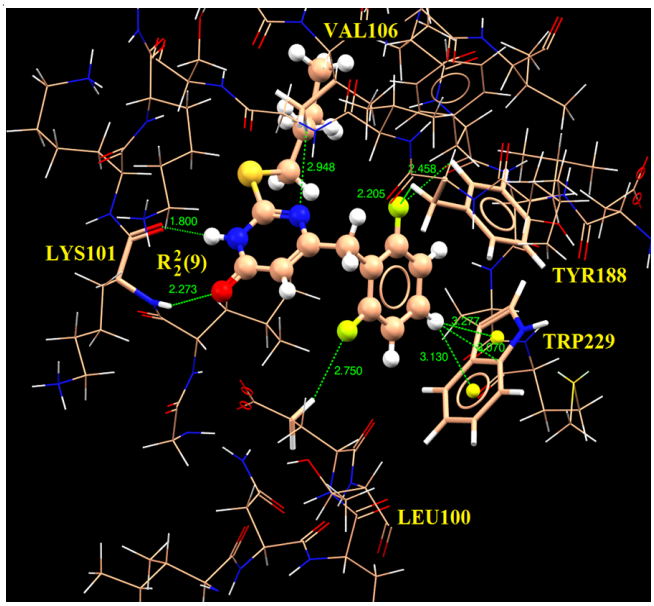

Fig. 8. Binding mode of molecule 42 at the active site of 1RT1 protein

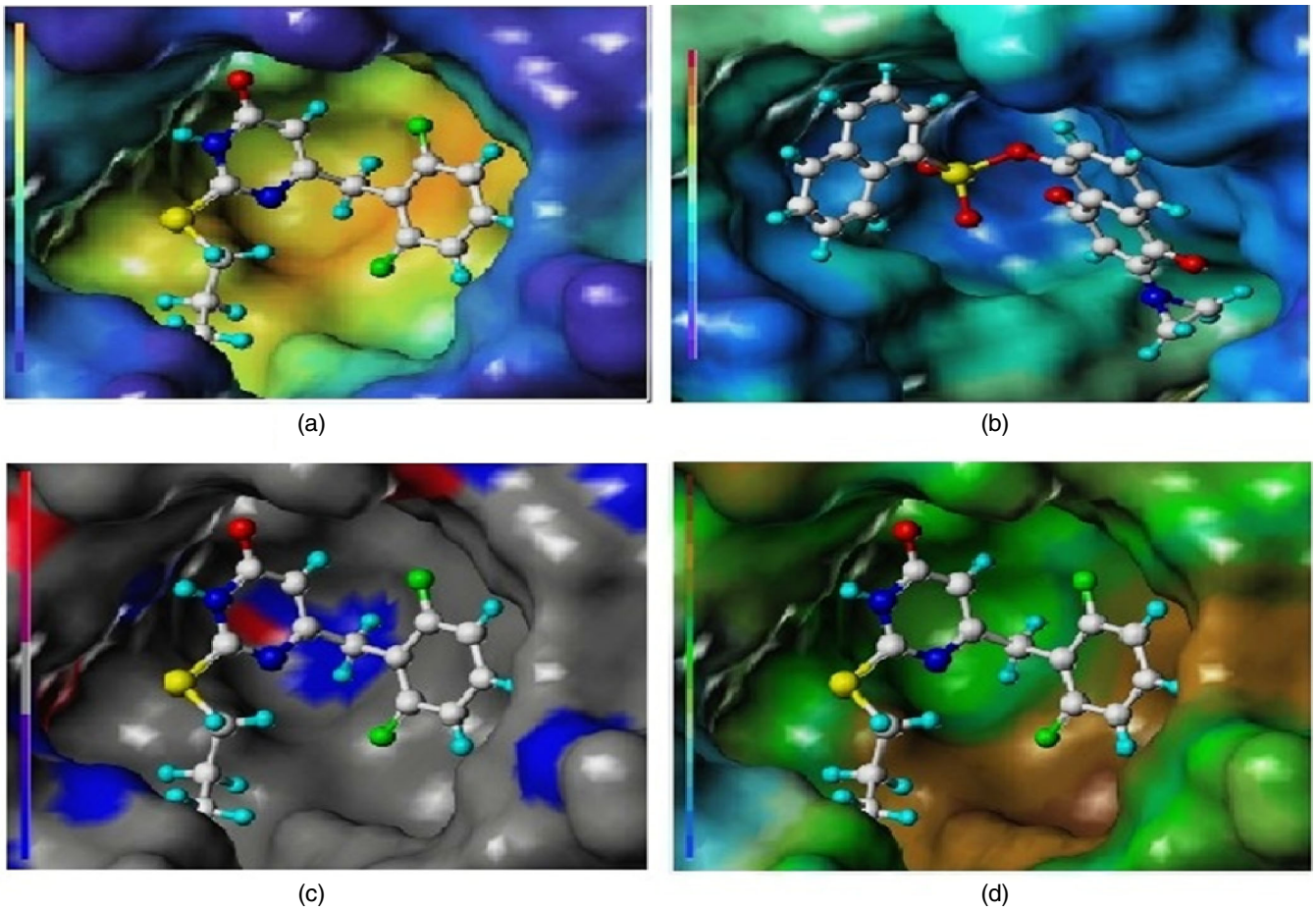

Fig. 9. MOLCAD surfaces of the binding site of 1RT1 protein with molecule 42. (a) Cavity depth (CD); colour ramp ranges from blue (low depth values, outside the pocket) to light red (high depth values deep, cavities deep inside the pocket); (b) Electrostatic potential (EP); colour ramp ranges from red (most positive) to purple (most negative); (c) Hydrogen bonding sites surface (HB); (d) colour ramp ranges from red (hydrogen bond)

The difluorobenzene moiety of the ligand 42 also interact with the surrounding protein residues (LEU100, TYR188 and TRP229). CH···F hydrogen bonding is established between the CH donor of LEU100 and the F acceptor on the ligand with C···F distance 3.42 Å, H···F distance 2.75 Å and <CH···F angle is 104.66°. Another CH···F hydrogen bonding is also established between the CH donor of TYR188 residue and the F acceptor on the ligand with C···F distance 2.86 Å, H···F distance 2.205 Å and <CH···F angle is 115.0°.

A CH···π hydrogen bonding is established between the terminal CH group of the difluorobenzene moiety and the TRP229 residue of the protein. The H···centroid of phenyl ring distance is 3.130 Å.

Further, the MOLCAD surfaces of the binding site of 1RT1 have been developed to show the hydrogen bonding sites (HB) (Fig. 9a), electrostatic potential (EP) (Fig. 9b), lipophilic potential (LP) (Fig. 9c) and cavity depth (CD) (Fig. 9d). The molecular electrostatic potential on a protein surface can be used to find the areas that act as attraction sites for the regions of the ligand having matching opposite colours. The red colour shows the electron-withdrawing zone and purple colour shows electron-donating zone. The interactions depicted for hydrogen bonding contacts in Fig. 8 correlate to that of the CoMFA electrostatic contour map.

Conclusion

3D-QSAR and docking studies have been performed to rationalize the cause of anti HIV-activity of a set of dihydro-alkoxybenzyloxopyrimidines (DABO) molecules whose activity values are known. 3D-QSAR has been formed using CoMFA and CoMSIA methods. The CoMFA analysis reveals that electrostatic field is more important than the steric field in case of anti-HIV activity of DABO molecules. Whereas less bulkysubstituents are preferred at the position of X, more electronegative subtituents at the periphery of the Ar substituent is likely to increase the anti HIV activity. CoMSIA analysis also indicate the same trend like the CoMFA analysis. A docking analysis has been performed which show that hydrogen bonding as well as π-stacking interactions are important for binding of the molecules with the HIV protein 1RT1. In the 3D-QSAR analysis, it was revealed that suitable donor groups on the protein will help in greater binding affinity of the dabo molecules, which have multiple acceptor sites. The docking analysis revealed that the core moiety of the DABO molecules have a nice donor acceptor complementary for binding with the lysine residue of a protein and forms a cyclic hydrogen bonding motif. The symmetrically positioned acceptors on the Ar group also suitably binds with different protein residues. In line with the CoMSIA analysis, in the docking study also it is revealed that besides the central core the Ar group is important for binding with the protein and should be carefully designed for better anti-HIV drug molecules. In summary, the present 3D-QSAR analysis clearly explains the observed anti-HIV activity of the DABO molecules. Insight obtained from this study should be helpful in designing more effective anti-HIV drug molecules.

ACKNOWLEDGEMENTS

One of the authors, ADJ acknowledges the financial support from the Department of Science, Technology and Biotechnology, Government of West Bengal, India through the project no ST/P/S&T/16G-47/2017.

REFERENCES

1. E. De Clercq, New Approaches Toward Anti-HIV Chemotherapy, *J. Med. Chem.*, **48**, 1297 (2005); https://doi.org/10.1021/jm040158k
2. H.C. Castro, N.I.V. Loureiro, M. Pujol-Luz, A.M.T. Souza, M.G. Albuquerque, D.O. Santos, L.M. Cabral, I.C. Frugulhetti and C.R. Rodrigues, HIV-1 Reverse Transcriptase: A Therapeutical Target in the Spotlight, *Curr. Med. Chem.*, **13**, 313 (2006); https://doi.org/10.2174/092986706775476089
3. J. Balzarini, Current Status of the Non-nucleoside Reverse Transcriptase Inhibitors of Human Immunodeficiency Virus Type 1, *Curr. Top. Med. Chem.*, **4**, 921 (2004); https://doi.org/10.2174/1568026043388420
4. E. De Clercq, HIV-Chemotherapy and -Prophylaxis: New Drugs, Leads and Approaches, *Int. J. Biochem. Cell Biol.*, **36**, 1800 (2004); https://doi.org/10.1016/j.biocel.2004.02.015
5. E. De Clercq, *Biochim. Biophys. Acta Mol. Basis Dis*, **1587**, 258 (2002); https://doi.org/10.1016/S0925-4439(02)00089-3
6. C. Flexner, ed.: L.L. Brunton, Antiretroviral Agents and Treatment of HIV Infection in Goodman & Gilman: The Pharmacological Basis of Therapeutics, McGraw Hill: New York, NY, edn. 12; Section VIII, Chap. 9, pp 1273-1314 (2006).
7. H.R. Xu, L. Fu, P. Zhan and X.Y. Liu, 3D-QSAR Analysis of a Series of S-DABO Derivatives as Anti-HIV Agents by CoMFA and CoMSIA, *SAR QSAR Environ. Res.*, **27**, 999 (2016); https://doi.org/10.1080/1062936X.2016.1233580
8. H. Kubinyi, G. Folkers and Y.C. Martin, 3D QSAR in Drug Design, Kluwer: Dordrecht (1988).
9. T. Puzyn, J. Leszczynski and M.T.D. Cronin, Recent Advances in QSAR Studies, Springer (2009).
10. R.D. Cramer, D.E. Patterson and J.D. Bunce, Comparative Molecular Field Analysis (CoMFA). 1. Effect of Shape on Binding of Steroids to Carrier Proteins, *J. Am. Chem. Soc.*, **110**, 5959 (1988); https://doi.org/10.1021/ja00226a005
11. I.A. Doytchinova and D.R. Flower, A Comparative Molecular Similarity Index Analysis (CoMSIA) Study Identifies an HLA-A2 Binding Supermotif, *J. Comput. Aided Mol. Des.*, **16**, 535 (2002); https://doi.org/10.1023/A:1021917203966
12. G. Klebe, U. Abraham and T. Mietzner, Molecular Similarity Indices in a Comparative Analysis (CoMSIA) of Drug Molecules to Correlate and Predict Their Biological Activity, *J. Med. Chem.*, **37**, 4130 (1994); https://doi.org/10.1021/jm00050a010
13. M. Batool, Protein Modelling & Molecular Docking, LAP Lambert Academic Publishing (2012).
14. R. Bathini, S.K. Sivan, S. Fatima and V. Manga, Molecular Docking, MM/GBSA and 3D-QSAR Studies on EGFR Inhibitors, *J. Chem. Sci.*, **128**, 1163 (2016); https://doi.org/10.1007/s12039-016-1103-3
15. A. Misra, S. Sharma, D. Sharma, S. Dubey, A. Mishra, D. Kishore and J. Dwivedi, Synthesis and Molecular Docking of Pyrimidine Incorporated Novel Analogue of 1,5-Benzodiazepine as Antibacterial Agent, *J. Chem. Sci.*, **130**, 31 (2018); https://doi.org/10.1007/s12039-018-1430-7
16. SYBYL-X 2.0, Tripos Inc, St. Louis.
17. A. Mai, M. Artico, G. Sbardella, S. Massa, A.G. Loi, E. Tramontano, P. Scano and P. La Colla, Preparation and Anti-HIV-1 Activity of Thio Analogues of Dichydroalkoxybenzyloxopyrimidines, *J. Med. Chem.*, **38**, 3258 (1995); https://doi.org/10.1021/jm00017a010
18. A. Mai, M. Artico, G. Sbardella, S. Quartarone, S. Massa, A.G. Loi, A. De Montis, F. Scintu, M. Putzolu and P. La Colla, Dihydro(alkylthio)-(naphthylmethyl)oxopyrimidines: Novel Non-Nucleoside Reverse Transcriptase Inhibitors of the S-DABO Series, *J. Med. Chem.*, **40**, 1447 (1997); https://doi.org/10.1021/jm960802y

19. A. Mai, M. Artico, G. Sbardella, S. Massa, E. Novellino, G. Greco, A.G. Loi, E. Tramontano, M.E. Marongiu and P. La Colla, 5-Alkyl-2-(alkylthio)-6-(2,6-dihalophenylmethyl)-3,4-dihydropyrimidin-4(3*H*)-ones: Novel Potent and Selective Dihydro-alkoxy-benzyl-oxopyrimidine Derivatives, *J. Med. Chem.*, **42**, 619 (1999); https://doi.org/10.1021/jm980260f
20. R. Ragno, A. Mai, G. Sbardella, M. Artico, S. Massa, C. Musiu, M. Mura, F. Marturana, A. Cadeddu and P. La Colla, Computer-Aided Design, Synthesis and Anti-HIV-1 Activity *in vitro* of 2-Alkylamino-6-[1-(2,6-difluorophenyl)alkyl]-3,4-dihydro-5-alkylpyrimidin-4(3*H*)-ones as Novel Potent Non-Nucleoside Reverse Transcriptase Inhibitors, also Active against the Y181C Variant, *J. Med. Chem.*, **47**, 928 (2004); https://doi.org/10.1021/jm0309856
21. M.D.M. Abdul-Hameed, A. Hamza, J. Liu and C.-G. Zhan, Combined 3D-QSAR Modeling and Molecular Docking Study on Indolinone Derivatives as Inhibitors of 3-Phosphoinositide-Dependent Protein Kinase-1, *J. Chem. Inf. Model.*, **48**, 1760 (2008); https://doi.org/10.1021/ci800147v
22. D.M. Hawkins, S.C. Basak and D. Mills, Assessing Model Fit by Cross-Validation, *J. Chem. Inf. Comput. Sci.*, **43**, 579 (2003); https://doi.org/10.1021/ci025626i
23. P.P. Roy and K. Roy, On Some Aspects of Variable Selection for Partial Least Squares Regression Models, *QSAR Comb. Sci.*, **27**, 302 (2008); https://doi.org/10.1002/qsar.200710043
24. G.R. Desiraju, Supramolecular Synthons in Crystal Engineering-A New Organic Synthesis, *Angew. Chem. Int. Ed. Engl.*, **34**, 2311 (1995); https://doi.org/10.1002/anie.199523111